

pubs.acs.org/JPCC Article

Impact of the Plasmonic Metal Oxide-Induced Photocatalytic Processes on the Interaction of Quantum Dots with Metallic Nanoparticles

Seyed M. Sadeghi,* Rithvik R. Gutha, and Waylin J. Wing



Cite This: J. Phys. Chem. C 2020, 124, 4261-4269



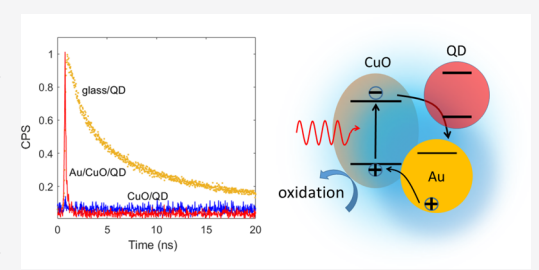
ACCESS

III Metrics & More



S Supporting Information

ABSTRACT: We study plasmonic control of photocatalytic properties of metal oxides and the ways they influence interaction of quantum dots with metallic nanostructures. For this, gold nanostructures are coated with ultrathin layers of metal oxides (Al, Cu, Cr, or Ti oxide) and then covered with CdSe/ZnS quantum dots. The results show how the photocatalytic properties of such metal oxides are renormalized by plasmon near fields. In the cases of Al, Cr, and Ti oxides, the results mostly indicate the direct impact of plasmon fields via enhancement of optical excitations of the quantum dots. For the case of Cu oxide, however, the outcomes are found to be quite unique. In the absence of the plasmonic structures, such an oxide (CuO) presents highly active



photocatalytic processes, leading to complete annihilation of the quantum dot emission. In the presence of the metallic nanostructures, the emission of such quantum dots is revived, offering an ultrafast decay process (~112 ps). These results indicate that in the case of CuO, the plasmonic metal oxide-induced photocatalytic processes include not only direct impact of plasmon near fields on the optical excitations of quantum dots but also the enhancement of interband transitions in CuO nanoparticles. The effects of energy transfer from quantum dots to metallic nanostructures and its equalization with Purcell effects on such processes are discussed.

1. INTRODUCTION

Significant interest has been devoted to the application of plasmonic properties of metallic nanoparticles (MNPs) to suppress or enhance the emission of the semiconductor quantum dots (QDs) and, in general, to control light-matter interaction. 1-8 Interactions of QDs with MNPs are influenced by two major factors: (i) the defect environments (DEs) of the QDs and (ii) the impact of plasmon near fields on their photophysical and photochemical properties. The DEs include surface and interfacial defects in QDs and the trap sites nested in the substrate. The extent of the DEs can significantly influence plasmonic emission enhancement factors of QDs $(P_{\rm enh})$, defined as the ratio of emission of QDs in the presence of MNPs to that in their absence. In the presence of a large number of defect sites (small quantum yields), one can expect large P_{enh} values, while under the same plasmonic settings when the defect sites are suppressed, these factors become smaller. Recently, we showed one can use plasmonic effects not only to enhance the near fields experienced by QDs but also to suppress their DEs. 9-11 This makes QDs unique superemitters by increasing their quantum yields by both the Purcell effect and the quarantine of their excitons against the substrate and surface defect sites.

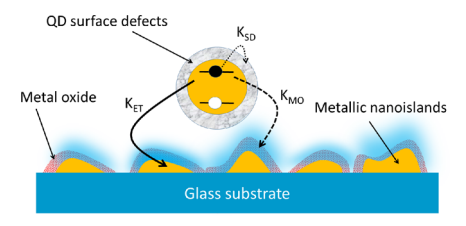
Photocatalytic properties of QDs are related to the way they react with the environment. A large number of reports have already demonstrated photopassivation and oxidation of QDs when they are exposed to light over a period of time in the absence ^{12–15} and presence of plasmonic effects. ¹⁶ Also recently, we studied the profound impact of metal oxides on the emission of QDs. ^{10,14,15,17,18} These include acceleration of their photo-oxidation by Cr oxide, ¹⁷ field effect enhancement of QD lifetimes by Si/Al oxide junction, ^{14,15} and suppression of plasmon-enhanced energy transfer between QDs. ¹⁹ Recent reports also include investigation of plasmonic photocatalysis wherein one uses localized surface plasmon resonances (LSPRs) of MNPs to enhance semiconductor photocatalytic efficiencies. This is done by utilizing hot electrons that are generated by the decays of plasmons, plasmonic heating effects, light scattering, and dipole—dipole interaction. ^{20–24}

In this paper, we study plasmonic metal oxide-induced photocatalytic processes and the way such processes influence the emission intensity and dynamics of QDs. This paper explores direct control of the DEs of QDs by metal oxides and the way interaction of such oxides with QDs is influenced by plasmonic effects. For this, we investigate the emission intensity and dynamics of QDs in the presence of metallic

Received: December 16, 2019 Revised: January 30, 2020 Published: February 3, 2020



nanoislands (NISs) when they are coated with an ultrathin layer of Al, Cr, Ti, or Cu oxide (Figure 1). These oxides offer a



K_{FT}: rate of FRET from QD to MNP

K_{sp.}: rate of photo-excited electron transfer to QD surface defects

 K_{MO} : rate of photo-exciton electron transfer to metal oxide

Figure 1. Schematic of Au NISs covered with metal oxide and QDs. The arrows denoted with $K_{\rm SD}$ and $K_{\rm MO}$ refer to the rate of transfer of photoexcited electrons to surface defects of QDs and the metal oxide, respectively. $K_{\rm ET}$ represents the rate of FRET from QDs to the NISs.

wide range of photocatalytic properties, ranging from weak to extremely high oxidation processes. Our results show that in the absence of NISs, Cu oxide can lead to complete annihilation of the QD emission. In the presence of NISs, however, the plasmon-field enhancement associated with LSPRs can revive the emission, offering ultrahigh plasmonic emission enhancement factor $(P_{\rm enh})$ in the presence of ultraactive DEs. We discuss these processes in terms of enhancement of light absorption in the Cu oxide (CuO) grains and a decrease in the emission decay rate of QDs by plasmonic effects (Purcell effect). The former leads to plasmon-assisted photocatalytic capabilities of CuO grains that distinguishes them from other the oxides.

To distinguish the defect-induced nonradiative decay processes from those that are not caused by the interaction of QDs with the DEs, in this paper we also provide a detailed discussion regarding Forster resonance energy transfer (FRET) from QDs to NISs and the Purcell effect. We demonstrate the limits wherein FRET can contribute dominantly to the nonradiative decay rates, and when this is compensated by the Purcell effect. Considering a broad range of sizes of NISs, we provide a metric for the impact of the sizes of NISs on such processes. This allows us to understand the role of defect-induced nonradiative decay in given plasmon settings. In particular, we also consider a structure that equalizes the contributions of FRET and Purcell effects and investigate how under this condition plasmonic effects modify the interaction of QDs with CuO nanoparticles.

2. METRICS OF NONRADIATIVE DECAY RATES VIA NONDEFECT EFFECTS

In the presence of metallic nanostructures, the loss processes in QDs are not limited to defect sites; rather, a main source of nonradiative decay can be FRET. Such a process is involved with the interaction of the QD dipoles with LSPRs. The level of contribution of this process is primarily determined by the sizes and shapes of the metallic nanostructures and their distances from QDs. The objective of this part of the paper is to obtain the metrics of contributions of FRET and the Purcell effect when the QDs are in contact with NISs. Such metrics allow us to distinguish the direct impact of plasmonic structures on QDs from those generated by plasmonically induced enhancement of photocatalysis of metal oxides.

Methodology. Metal oxide plasmonic structures were fabricated by evaporating gold onto glass substrates followed by their thermal annealing at 500 °C for 30 min. We decreased the thickness of the Au layers from 13 nm to a thickness (5 nm) at which the NISs had very small measurable effects. Panels a and d of Figure 2 show the scanning electron microscopy (SEM) images of NISs associated with these limits, respectively. Figure 2a was obtained after deposition of 13 nm of Au and Figure 2d after 3 nm of Au. Panels b and c of Figure 2 show the SEM images of the NISs associated with two typical intermediate steps between these limits with mass thicknesses of ~10 and ~6 nm of Au, respectively. We used a transmission optical setup to measure the extinction spectra of such samples and an Olympus microscope to obtain their dark-field backscattering spectra. After such characterization, CdSe/ZnS QDs, acquired from NN Laboratories LLC, were directly spin coated on the top of NISs. These QDs were optically excited by a 514 nm laser with a 2 mW power, emitting efficiently at 660 nm. The emission spectra of such QDs were measured using a spectrometer, and for their decay, we used a timecorrelated single-photon counting (TCSPC) system (Picoquant Pico-Timeharp 260).

Figure 3a shows that the extinction spectrum of NISs with the largest sizes (Figure 2a) has the highest amplitude (line 1). As the sizes of the NISs are decreased, the amplitude of the spectrum is decreased while it becomes narrow and blue-shifted. For the case of Figure 2d, the amount of extinction is rather quite small (line 4). This can be seen more vividly in Figure 3b wherein we compare the normalized extinction spectra for different sizes of NISs. The results show that for the largest NISs (line 1) the full width at half-maximum (fwhm) of the extinction spectrum is ~150 nm. For NISs shown in Figure 2d, the fwhm decreases to ~90 nm (line 4). This suggests, as shown in Figure 2d, smaller NISs tend to have more uniform sizes and shapes. Because the peak of the extinction spectrum associated with line 1 occurs at ~590 nm and that of line 4

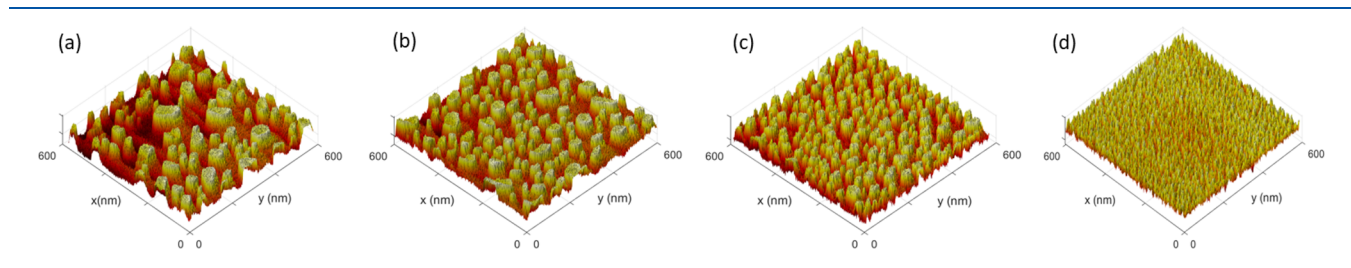


Figure 2. SEM images of Au NISs when the thicknesses of evaporated Au are (a) ~13, (b) 10, (c) 6, and (d) 3 nm. On the basis of their extinction spectrum peak wavelengths (Figure 3a), panels a and d are termed the Au590 and Au540 samples, respectively.

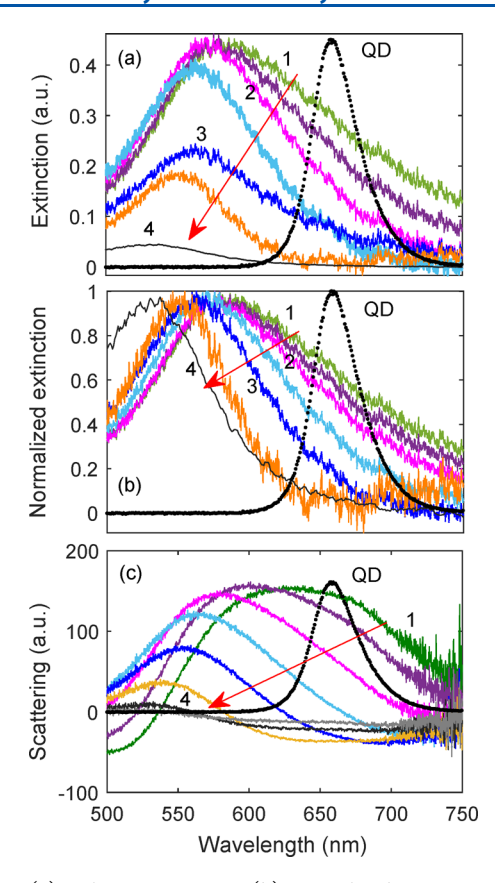


Figure 3. (a) Relative extinction, (b) normalized extinction, and (c) scattering spectra of the NISs as the shapes and sizes are changed from Figure 2a (line 1) to Figure 2d (line 4). Lines 2 and 3 refer to the spectra associated with Au mass thicknesses of ~ 10 nm (Figure 2b) and 6 nm (Figure 2c), respectively. The arrows represent the trend of the decrease in NIS size. The dotted spectra represent the emission spectrum of the CdSe/ZnS QDs.

happens at 540 nm, in the following we refer to the plasmonic structures associated with lines 1 (Figure 2a) and 4 (Figure 2d) as Au590 and Au540 samples, respectively.

The corresponding dark-field backscattering spectra of the NISs were also measured perpendicular to the surface of the substrates. The results in Figure 3c show that for NISs associated with Figure 2a the scattering spectrum is wide and has a relatively high amplitude (line 1). Additionally, the peak wavelength is ~630 nm, supporting a spectral line shape different from that of the extinction (Figure 3a, line 1). As the sizes of NISs are decreased, however, the scattering spectrum undergoes a significant amount of blue shift and suppression of amplitude. In fact, line 4 in Figure 3c represents the case of NISs in Figure 2d with nearly no scattering. The results in Figure 3c show that the scattering spectra for certain sizes of NISs can become negative. This is an indication of the absorptive character of the small NISs. In fact, as previously shown, 25 absorption is more dominant for small NISs. The narrow spectra centered around 660 nm (black dot) in these figures refer to the emission spectra of CdSe/ZnS QDs, demonstrating the amount of overlap it has with the extinction and scattering spectra.

Scaling of the Purcell Effect and FRET. To investigate the scales of the contributions of FRET and the Purcell effect, we specifically study the emission intensity and dynamics of QDs spin coated on the NISs shown in panels a (Au590

sample) and d (Au540 sample) of Figure 2. Under these conditions, the QDs are in contact with the NISs. Such a system offers a convenient test bed for investigation of plasmon-induced photocatalytic processes involving QDs. The results in Figure 4a show that, compared to the QDs on glass

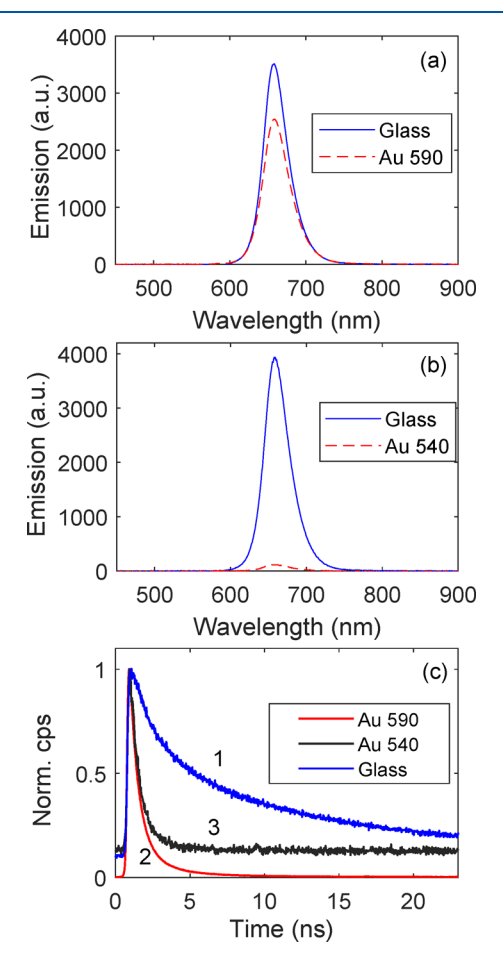


Figure 4. Emission spectra of CdSe/ZnS QDs in the absence (solid line) and presence (dashed line) of NISs for (a) Au590 and (b) Au540 samples. (c) Decay of such QDs on glass (line 1), Au590 (line 2), and Au540 (line 3). In panel c, cps refers to counts per second.

(solid line), for the case of the Au590 sample (largest NISs) we see an only modest reduction in emission intensity (dashed line). For the case of the Au540 sample (smallest NISs), however, the emission of QDs decreases dramatically, by ~35 times (Figure 4b). The results presented in Figure 4c show that the decay of QDs in the absence of NISs, i.e., on glass, depicts their typical lifetime (line 1). In the presence of NISs, however, for both samples we see rather faster decay processes. As discussed in detail in section 4, the decay in the case of Au540 sample is mostly caused by ultraefficient FRET loss of the QDs (line 3). This process overwhelmingly influences the decay process, as indicated by the near complete reduction of emission within the initial few nanoseconds. In the case of the Au590 sample, however, the combination of FRET and the Purcell effect plays the key role. The combined impact of these processes can be seen as a relatively longer decay, reaching \sim 10 ns (line 2), as the radiative decay process here plays a more important role.

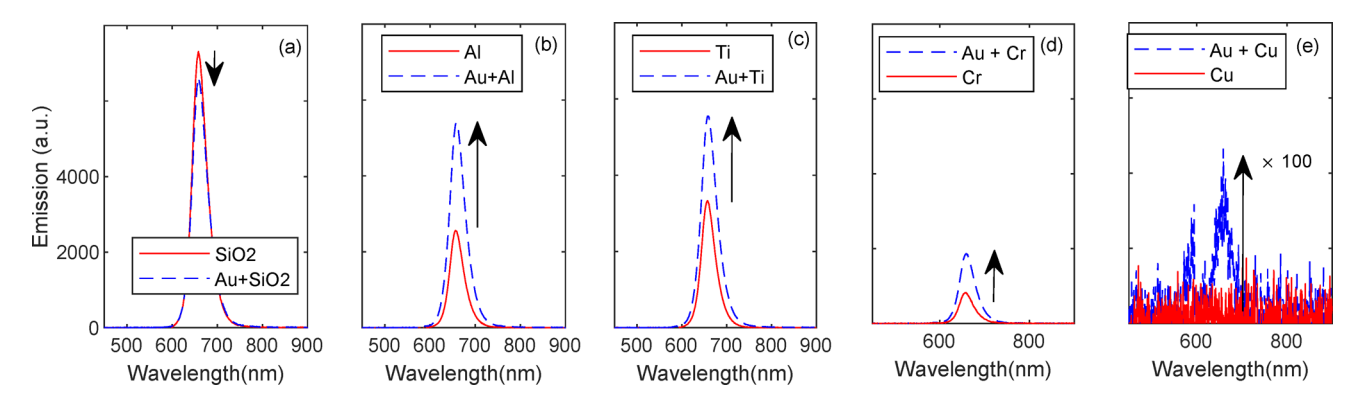


Figure 5. Emission spectra of CdSe/ZnS QDs on (a) SiO₂, (b) Al oxide, (c) Ti oxide, (d) Cr oxide, and (e) Cu oxide in the absence (solid lines) and presence of the NISs as shown in Figure 2a (dashed lines).

3. PHOTOCATALYTIC DESIGN OF THE DEFECT ENVIRONMENT OF OUANTUM DOTS

The results in the preceding section highlighted the competition between FRET and the Purcell effect when QDs were in contact with the NISs. Such a process is influenced by the presence of the DEs. An important feature of metal oxides is that they can change the DEs via introduction of new defect sites and certain photocatalytic processes. In the presence of NISs, we expect such processes are influenced by plasmonic effects, which can, in turn, reshape the DEs. Primarily, such processes are related to the plasmon near fields, which can renormalize the interaction between the metal oxides and the QDs.^{26,27} In fact, as shown in the following, such fields can modify the photocatalytic processes of metal oxides in two ways: (i) via increasing the excitation rates of QDs and (ii) enhancement of their photo-oxidation capabilities. To investigate these, we coated the NISs shown in Figure 2a (Au590) with various metal oxides. For this, we sputtered 1 nm of Al, Cu, Ti, or Cr on these NISs and then exposed them to air, forming oxides (air oxidation). These steps were followed by spin coating of the CdSe/ZnS QDs on the top of the oxides. Different reference samples were also fabricated. These include samples consisting of glass substrates with and without NISs coated with 1 nm of SiO₂. They also include samples in which metal oxides were deposited on glass substrates (no NISs). Note that the air oxidation process of metals has been studied in the past extensively. ²⁸⁻³¹ These include, in particular, oxidation of Cu oxide and its characterization under conditions similar to those adopted in this paper. ^{29,31-33} Panels a-e of Figure 5 show the emission of QDs on the SiO₂, Al oxide, Ti oxide, Cr oxide, and Cu oxide layers, respectively, in the absence (solid lines) and presence (dashed lines) of NISs. The results in Figure 5a show that with the nanometer SiO₂ coating, the presence of NISs reduces the emission of QDs slightly. This is quite different from the case for samples with metal oxides. In fact, as shown in panels b and c of Figure 5, in the cases of Al and Ti oxides, NISs lead to the enhancement of QD emission. For the case of Cr oxide (Figure 5d), a similar situation occurs, although the QD emission is found to be much less than those of the Al and Ti oxides. Samples with Cu oxide, on the other hand, offer a quite different picture. In the absence of NISs, i.e., QDs on glass covered with Cu oxide, the emission of the QDs is completely annihilated (Figure 5e). Introduction of the NISs, however, revives the emission of the QDs to some extent.

The results shown in Figure 5 can be associated with the effects of SiO₂ and the metal oxides on the DEs of the QDs and the way these effects are renormalized by plasmons. To analyze these further, in panels a and b of Figure 6, we study

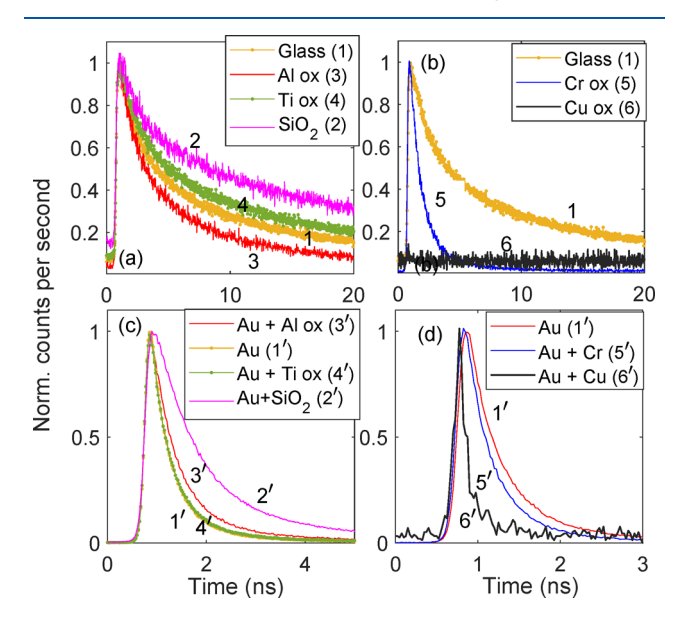


Figure 6. Decay of QDs (a) on glass covered with 1 nm of SiO₂ (line 2), Al oxide (line 3), and Ti oxide (line 4), (b) on Cr oxide (line 5) and Cu oxide (line 6), (c) on Au/SiO₂ (line 2'), Au/Al oxide (line 3'), and Au/Ti oxide (line 4'), and (d) on Au/Cr oxide (line 5') and Au/Cu oxide (line 6'). Here the Au sample had NISs like those shown in Figure 2a (Au590). Lines 1 and 1' show the results when QDs were directly spin coated on glass substrate and NISs (no oxide), respectively.

the emission dynamics of QDs in the absence of NISs. The results in Figure 6a show that adding SiO_2 (line 2) significantly enhances the lifetime of QDs compared to the lifetimes of those directly deposited on glass substrates (line 1). For the case of Al oxide, we see a decrease in lifetime (line 3), while for Ti oxide, a slight lifetime elongation occurs (line 4). As shown in Figure 6b, suppression of the QD emission lifetime in the presence of Cr oxide is rather quite significant (line 5). In the presence of Cu oxide, there are literally no photon counts or detects (line 6), as also shown in Figure 5e.

Line 1' in Figure 6c shows that the decay of QDs when they were directly placed atop the NISs. The time scale of this decay is more or less similar to those of the QDs when they were

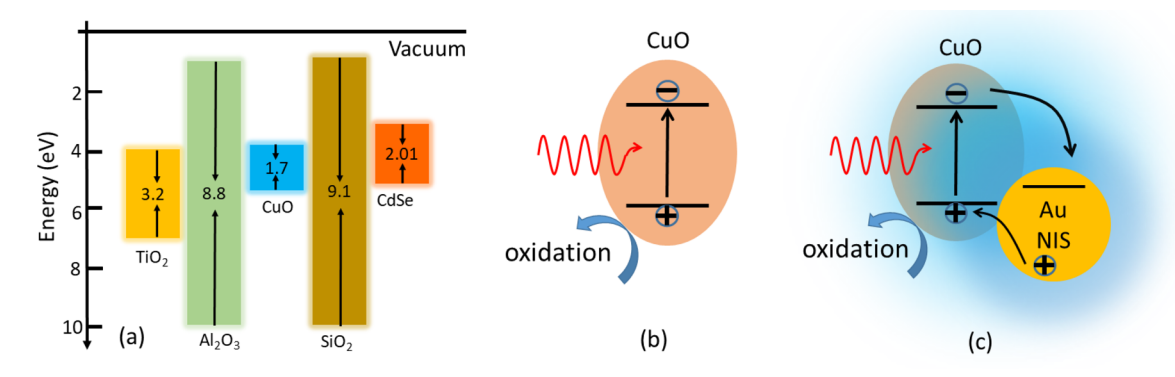


Figure 7. (a) Bandgap energies of Al, Cr, Ti, and Cu oxides and CdSe. The data are taken from refs 47 (CdSe and Ti oxide), 35 (CuO), and 44 (Al,O₃). Photocatalytic process of a CuO nanoparticle (b) on glass and (c) in the presence of Au NISs.

separated from NISs with Al oxide (line 3') and Ti oxide (line 4'). In the case of SiO₂ (line 2'), however, the decay rate is slowest. Figure 6d compares the emission decays of the QDs when they were separated from the NISs with Cr oxide (blue line 5') and Cu oxide (black line 6') and when they were directly deposited on NIS (red line 1'). The case of Cu oxide indicates two important observations. First, the presence of Au NISs allows the emission of the QDs to become visible, confirming the results presented in Figure 5e. Second, the decay of QDs on Cu oxide seems to happen over a very short period of time.

Note that, in the absence of NISs, the results in panels b and c of Figure 5 (solid lines) show that the emission of QDs is less than half of those on glass substrates covered with 1 nm of SiO₂ (Figure 5a). This can be associated with the surface passivation by the SiO₂ layer. ¹⁸ In fact, because SiO₂ has a very large bandgap (Figure 7a), it prevents migration of photoexcited electrons from QDs to defect sites in the substrate, leading to higher emission and longer lifetimes (Figure 6a, line 2). Additionally, our previous reports have shown that when QDs are spin coated on an ultrathin layer of Al oxide (0.5-1 nm) deposited on the top of a Si layer, they can become brighter with longer lifetimes. This is due to the surface charges formed at the Si/Al oxide interface.³⁴ In the cases studied here, however, the Al oxide layers were deposited on the glass substrate, introducing some defects, instead. This explains the faster decay seen in Figure 6a (line 3). For the case of Cr oxide, the sharp decrease in lifetime seen in Figure 6b (line 5) can be associated with the defects generated by the oxidation of ZnS shells and CdSe cores of the QDs. 17

The case of Cu oxide, however, seems to be quite unique. It is well-known that Cu nanoparticles can easily be oxidized under ambient conditions. 35-38 Additionally, when an ultrathin layer of Cu is exposed to air, as shown in ref 29, the primary oxide is CuO. It has been shown that such an oxide is promising for photocatalytic hydrogen production, 39,40 as a catalyst for different types of materials, 41 and for sensing applications. ⁴² A key feature of CuO, compared to other oxides considered in this paper, is its bandgap. ^{35,43,44} As shown in Figure 7a, the bandgaps of Cr, Ti, and Al oxides are all significantly larger than that of QDs. In the case of CuO, however, the bandgap energy falls within the visible range.³⁵ Therefore, the incident light can cause an interband transition in such an oxide, generating electron and hole pairs (Figure 7b). This allows CuO to generate a photolysis process wherein water molecules split via holes. This process causes formation of active OH radicals, causing oxidation. 45,46

Considering this, deposition of 1 nm of Cu should lead to formation of small grains of CuO that are a few nanometers in size. Therefore, the annihilation of the QD emission in the absence of NISs, as shown in Figures 5e and 6b (line 6), can be attributed to their strong photo-oxidation by such oxide nanoparticles (Figure 7b). This process significantly modifies the DEs of the QDs, offering more defect trap sites for the photoexcited electrons in their cores. This leads to ultrafast nonradiative decay processes that can overwhelm the radiative decay of the QDs and annihilate their emission.

To consider the impact of plasmonic effects, note that the results in Figure 6c show that the decay of QDs on SiO₂ (line 2') is far slower than the decay of those directly placed on NISs (line 1'). This can be associated with the separation between the QDs and NISs, which leads to a reduction of FRET, and also with the fact that the SiO₂ layer presents a barrier for charge transfer from QDs to the substrate. For the cases of Ti and Al oxides in the presence of NISs, the results in Figure 6c suggest decay time scales close to those of QDs that were directly spin coated atop the NISs (lines 1', 3', and 4'). This indicates a lack of interaction between these oxides and the plasmonic effects. In fact, here the plasmons can mostly intensify the fields experienced by the QDs. This, in turn, can enhance their photo-oxidation by such oxides.

For the case of CuO nanoparticles, however, the situation is different. Previous reports have shown that Au nanoparticles can enhance the photocatalytic properties of CuO. 42,51,52 Such a process has been used for degradation of organic contaminants⁵¹ and enhancement of sensing applications of CuO. 42,52 The results depicted in Figures 5e and 6d (line 6'), therefore, highlight how under such conditions Au NISs can revive the emission of QDs. In fact, as shown schematically in Figure 7c, the NISs can enhance the photocatalytic properties of CuO grains in two ways. The first is enhancement of their excitation rates via plasmonic near fields.⁵³ The second is related to the junction between CuO and NISs, which may allow transfer of holes from Au NISs to CuO. 54 This issue will be discussed further in section 5. Overall, these results suggest that despite the presence of strong plasmon-enhanced photocatalysis of CuO nanoparticles, the emission of QDs can be partially revived via the Purcell effect. One expects if smaller NISs are used, FRET plays a more major role and the impact of CuO is changed. This will be discussed further in the following section. Additionally, the fact that the emission peak seen in Figure 5e is ~660 nm, i.e., lack of blue shift, suggests that the oxidation processes mostly damage the ZnS shells of the QDs.

Note that the increase in the thicknesses of the metal oxides studied in this paper had a wide range of impacts. In the case of Al oxide, as shown in the Figure S1, we noticed this can lead to significant reduction of emission intensity of QDs and shortening of their lifetimes. This happens up to a certain thickness (~5 nm), after which the emission starts to increase as the Al thickness goes beyond its oxide thickness. ¹⁰ In the case of Ti oxide, however, we observed a more inert impact (Figure S2). Our previous report has highlighted the impact of thickness of Cr oxide, which includes significant reduction of emission intensity. ⁵⁵

4. ANALYSIS OF QD EMISSION DYNAMICS

To discuss the results presented in the preceding section further, we describe the emission decay of QDs using a biexponential function as 56,57

$$I(t) = C_{\rm f} e^{-t/\tau_{\rm f}} + C_{\rm s} e^{-t/\tau_{\rm s}}$$
(1)

where $C_{\rm f}$ and $\tau_{\rm f}$ refer to the amplitude and decay time of the fast processes, respectively, and $C_{\rm s}$ and $\tau_{\rm s}$ to those of the slow processes. The fast processes are related to nonradiative decay of QDs, and the slow processes to radiative decay of QDs. ^{58–61} The results of the fittings are listed in Table 1. For the case of

Table 1. Results of the Biexponential Fitting $(eq 1)^a$

	$\tau_{\rm f}~({\rm ns})$	$\tau_{\rm s}$ (ns)	$C_{\rm f}/C_{\rm s}$
glass (line 1)	2.25	19	1.3
Al oxide (line 3)	2.05	13.5	2
Au590 (line 1')	0.38	1.92	11.8
Au540 (line 3)	0.68	200	5.85
Au/Al oxide (line 3')	0.54	4.22	19
Au/Cu oxide (line 6')	0.112	235	19

^aThe line numbers refer to those shown in Figure 6, expect for the case of the Au540 sample in Figure 4c.

QDs on glass, these results suggest that $\tau_f = 2.25$ and $\tau_s = 19$ ns. The shorter lifetime associated with the fast processes and the fact that $C_f/C_s = 1.3$ suggest the extent of the contribution of defects and electron transfer to the surface or interfacial defects of the QDs. K_{SD} in Figure 1 represents the combined rate of such processes. S8,59 In addition to these, because we are dealing with QD thin films, the defect sites nested in the substrate can also contribute to the fast processes (nonradiative decay) efficiently.¹⁴ In the presence of metal oxide layers, extra channels of decay are formed via transfer of electrons to the defect sites in these layers (K_{MO} in Figure 1). In the case of CuO, this totally overwhelms the emission of QDs, making them dark (Figure 5e). To show the impact of metal oxides on QDs, in general, here we consider the case of a glass substrate covered with Al oxide (Figure 6a, line 3). Table 1 shows under this condition τ_f decreases to ~2.05 ns and C_f / C_s becomes ~ 2 . This indicates that the Al oxide layer introduces a wider range of defects. These defects are partially due to the fact that such a layer is prepared by exposing Al layers to the ambient environment, and therefore, they contained high densities of open volume defects.⁶²

The results in Table 1 also highlight the impact of FRET and the Purcell effect. For this, note that for the case of QDs on Au590 (Figure 6c, line 1') we have a $\tau_{\rm f}$ of 380 ps and a $\tau_{\rm s}$ of 1.92 ns. Additionally the value of $C_{\rm f}/C_{\rm s}$ becomes ~11.8. Comparing these results with those of QDs on glass suggests significant slowing of both fast and slow processes. The

decrease in τ_s can be partially associated with near fields of the plasmons or enhancement of the radiative decay rates of QDs (Purcell effect). On the other hand, the decrease in τ_f is the result of FRET, and perhaps introduction of some extra defect sites.

To support this in section 2 of the Supporting Information, we provided some data that show how the extinction spectra of Au NISs are shifted with variation of the refractive index of the superstate (Figures S3 and S4). In section S3 of the Supporting Information, we present a model that accounts for the interaction of Au NISs with QDs as the refractive index of the environment is varied. The results depicted in Figure S6 show the contributions of the plasmon-field enhancement factor (P_{enh}) and the rate of FRET (K_{ET}) from QDs to metallic nanoparticles with two very different sizes. The results depicted in panels a-c of Figure S6 highlight the physics behind Figure 4a (Au590), while the results depicted in panels a'-c' of Figure S6 represent the case associated with the Au540 sample (Figure 4b). These results show that for the case large metallic nanoparticles, $P_{\rm enh}$ and $K_{\rm ET}$ are both significant, suggesting an efficient competition between the Purcell effect and FRET. For the case of small nanoparticles, however, K_{ET} remains strong (Figure S6c'), but the values of $P_{\rm enh}$ are insignificant. These results highlight the role of NISs in the Au540 sample as an efficient FRET center that significantly suppresses the emission of QDs (Figure 4b, dashed line). In fact, the results of fitting to Figure 4c for the case of Au540 (line 3), as shown in Table 1, suggest a τ_s of ~200 ns and a τ_f of 680 ps. Therefore, although here $C_{\rm f}/C_{\rm s}$ is ~5.85, the nonradiative decay of the QDs is quite overwhelming.

For the case of CuO, the complete suppression of emission of QDs made them undetectable even for the avalanche single-photon detector of our TCSPC system (Figure 6b, line 6). Table 1 shows the results of the fitting to Au/Cu oxide decay shown in Figure 6d (line 6'). For this case, we are dealing with the case that is the result of combination of FRET and the Purcell effect with the ultrafast nonradiative decay associated with CuO nanoparticles. The results of the fitting suggest a $\tau_{\rm f}$ of 112 ps, a $\tau_{\rm s}$ of 235 ns, and a $C_{\rm f}/C_{\rm s}$ of 19. The ultrafast nonradiative decay seen here suggests that FRET from QDs to NISs, under these conditions, does not play a prominent role. Therefore, the increase in emission in Figure 5e can be associated with the Purcell effect, which in the case of the Au590 sample is strong.

5. PHOTOCATALYTIC PROPERTIES OF CUO NANOPARTICLES UNDER BALANCED PLASMONIC EFFECTS

The results presented in Figure 4a (dashed line) show that when QDs are in contact with NISs the Purcell effect can partially compensate for the impact of FRET, leading to an emission that is \sim 75% of those on glass. This suggests a prominent rate of FRET (Figure S6b,c). To study the impact of plasmonic fields on the photocatalytic properties of Cu oxide further, here we equalize the impact of FRET and the Purcell effect. This can be done by making the emission of the QDs in the presence and absence of plasmonic structure similar using a SiO₂ spacer. This allowed us to minimize the migration of the photoexcited electrons from the QD cores to the substrate while still having a significant impact of both FRET and the Purcell effect. For the case of NISs, as shown in Figure S7, our results show rather steep variations of the plasmonic emission enhancement factor (PEF) of QDs with

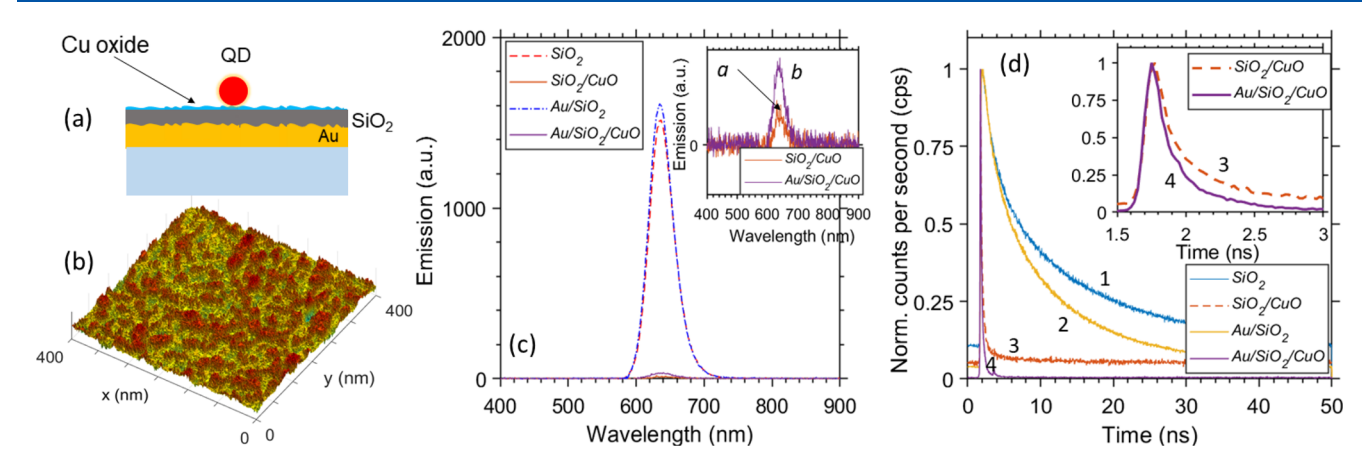


Figure 8. (a) Plasmonic structure with a balanced contribution of FRET and the Purcell effect. (b) Three-dimensional profile of the SEM image of the interface of the Au thin film in panel a. (c and d) Emission spectra and decay of QDs, respectively, in the presence of SiO_2 , SiO_2/CuO , Au/SiO_2 , and $Au/SiO_2/CuO$.

the sizes of the NISs. For this reason, we considered a structure consisting of a 40 nm Au thin film sputtered on a glass substrate, 15 nm of SiO₂, and 1 nm of Cu (Figure 8a). The QDs were then spin coated atop the CuO nanoparticles. The Au thin film had a rough surface, as shown in Figure 8b. Figure 8c (dashed and dotted—dashed lines) shows the key feature of such a structure wherein, in the absence of CuO, the QD emission intensities in the presence and absence of the Au thin film are very similar. This suggests that the reduction of emission caused by FRET is mostly compensated by the enhancement of emission via the near field of the Au thin film (Purcell effect).

The balanced contributions of FRET and the Purcell effect offer us unique grounds for assessing the impact of plasmonic effects on the photocatalytic properties of CuO nanoparticles. This is because under these conditions variations in the emission of the QDs in the presence of such an oxide can be nearly solely associated with its photocatalytic impact on QDs and the way plasmon fields influence such an impact. The results presented in the inset of Figure 8c show that when the CuO is deposited on SiO2 the emission of QDs can be detected, even when the plasmonic structure does not exist (line a). This, again, highlights the impact of SiO₂ in blocking migration of photoexcited electrons from QDs to the glass substrate. In the presence of the Au thin film, however, the emission of QDs is increased by a factor of \sim 2 (line b). This can be explained considering the fact that in the presence of CuO the quantum efficiencies of the QDs become significantly small. This allows the plasmonic emission enhancement factor to become >1. Lines 1 and 2 in Figure 8d compare the decay of QDs on SiO₂ and Au/SiO₂, respectively.

The results in Figure 8d suggest that when QDs are deposited on SiO_2/CuO their emission decay (line 3) becomes significantly faster than those that are directly spin coated on SiO_2 (line 1). To study this further, we used eq 1 to analyze the fast and slow components of the QD decay in these cases. For the case of QDs on SiO_2 (line 1), we obtained a C_f/C_s of 0.5 indicating a relatively low abundance of defect sites available to QDs. Note that when the QDs were directly deposited on glass (Figure 4c, line 1) this ratio was ~1.3. The results of fitting to line 1 in Figure 8d also show a τ_f of ~5 and a τ_s of 38 ns. For the case of QDs on SiO_2/CuO (line 3), however, we found a C_f/C_s of ~10, indicating an overwhelming increase in the number of defect sites available to QDs. Under

these conditions, we found a $\tau_{\rm f}$ of ~275 ps and a $\tau_{\rm s}$ of 155 ns, highlighting formation of ultrafast nonradiative decay via oxidation of QDs. The key feature of these results is that, because the SiO₂ layer isolated QDs from the substrate to some extent, they provide a better representation of the impact of the CuO nanoparticles.

As the inset of Figure 8d shows, the decay of QDs on CuO nanoparticles with the underlayer of the Au thin film (line 4) offers an even shorter lifetime than that on SiO₂/CuO. This suggests a decay process that is orders of magnitude faster than FRET on Au/SiO₂ (line 2). Therefore, because the direct impact of the Purcell effect on the QDs is compensated by the FRET effect, the increase in emission in Figure 8 (inset, line b) can be associated with the way the plasmon-field enhancement influences the CuO nanoparticles. Although here the amount of plasmonic enhancement of CuO photocatalytic properties is not like that in the case in which QDs were in touch with CuO-coated NISs, it is enough to cause a decrease in the lifetime of QDs (Figure 8d, inset, line 4). Additionally, a key feature of the structure considered in Figure 8 is the lack of a Au/CuO junction. Therefore, these results indicate that the impact of hole transfer from Au to such an oxide should be negligible.

6. CONCLUSIONS

We studied the impact of plasmon fields on the photocatalytic properties of metal oxides and the ways they influence the emission intensity and dynamics of QDs. For this, the metric of competition between FRET and plasmon-field enhancement spontaneous emission of QDs was explored. Such a metric allowed us to balance the contributions of FRET and the Purcell effect to the emission of QDs, paving the way for a more specific identification of the impact of Purcell effects on the photocatalytic properties of metal oxides. We studied four types of metal oxides, demonstrating while Al, Cr, and Ti oxides can cause limited photocatalytic processes, the impact of CuO is quite unique. We demonstrated that the key effect of CuO nanoparticles is related to their interband bandgap energies that facilitate photo-oxidation, leading to their complete annihilation of QD emission. In the presence of plasmonic effects, the enhancement of the interband excitations in CuO nanoparticles can make the ultrafast decay QDs caused by such an oxide even shorter, reaching \sim 250 ps.

ASSOCIATED CONTENT

Supporting Information

The Supporting Information is available free of charge at https://pubs.acs.org/doi/10.1021/acs.jpcc.9b11611.

Impact of metal oxide thickness on the dynamics of emission of QDs, variation of the emission enhancement factor with the thickness of SiO₂, wavelength shift of extinction spectra of NISs with refractive index, and modeling of plasmon-field enhancement of the rate of FRET from QDs to NISs (PDF)

AUTHOR INFORMATION

Corresponding Author

Seyed M. Sadeghi — Department of Physics and Astronomy, University of Alabama in Huntsville, Huntsville, Alabama 35899, United States; oorcid.org/0000-0002-5043-5032; Email: seyed.sadeghi@uah.edu

Authors

Rithvik R. Gutha — Department of Physics and Astronomy, University of Alabama in Huntsville, Huntsville, Alabama 35899, United States; oorcid.org/0000-0001-6172-2486

Waylin J. Wing – Department of Physics and Astronomy, University of Alabama in Huntsville, Huntsville, Alabama 35899, United States

Complete contact information is available at: https://pubs.acs.org/10.1021/acs.jpcc.9b11611

Notes

The authors declare no competing financial interest.

ACKNOWLEDGMENTS

This work is supported by U.S. National Science Foundation Grant ECCS-1917544.

REFERENCES

- (1) Biteen, J. S.; Pacifici, D.; Lewis, N. S.; Atwater, H. A. Enhanced radiative emission rate and quantum efficiency in coupled silicon nanocrystal-nanostructured gold emitters. *Nano Lett.* **2005**, *5*, 1768–1773.
- (2) Komarala, V. K.; Bradley, A. L.; Rakovich, Y. P.; Byrne, S. J.; Gun'ko, Y. K.; Rogach, A. L. Surface plasmon enhanced Förster resonance energy transfer between the CdTe quantum dots. *Appl. Phys. Lett.* **2008**, *93*, 123102.
- (3) Ito, Y.; Matsuda, K.; Kanemitsu, Y. Mechanism of photoluminescence enhancement in single semiconductor nanocrystals on metal surfaces. *Phys. Rev. B: Condens. Matter Mater. Phys.* **2007**, *75*, No. 033309.
- (4) Okamoto, K.; Vyawahare, S.; Scherer, A. Surface-plasmon enhanced bright emission from CdSe quantum-dot nanocrystals. *J. Opt. Soc. Am. B* **2006**, 23, 1674–1678.
- (5) Anger, P.; Bharadwaj, P.; Novotny, L. Enhancement and quenching of single-molecule fluorescence. *Phys. Rev. Lett.* **2006**, *96*, 113002.
- (6) Kühn, S.; Håkanson, U.; Rogobete, L.; Sandoghdar, V. Enhancement of single-molecule fluorescence using a gold nanoparticle as an optical nanoantenna. *Phys. Rev. Lett.* **2006**, 97, No. 017402.
- (7) Ma, X.; Tan, H.; Kipp, T.; Mews, A. Fluorescence enhancement, blinking suppression, and gray states of individual semiconductor nanocrystals close to gold nanoparticles. *Nano Lett.* **2010**, *10*, 4166–4174.

- (8) West, R.; Sadeghi, S. Enhancement of energy transfer between quantum dots: the impact of metallic nanoparticle sizes. *J. Phys. Chem.* C **2012**, *116*, 20496–20503.
- (9) Sadeghi, S. M.; Wing, W. J.; Gutha, R. R.; Sharp, C. Semiconductor quantum dot super-emitters: spontaneous emission enhancement combined with suppression of defect environment using metal-oxide plasmonic metafilms. *Nanotechnology* **2018**, 29, No. 015402.
- (10) Sadeghi, S. M.; Wing, W. J.; Gutha, R. R.; Wilt, J. S.; Wu, J. Z. Balancing silicon/aluminum oxide junction for super-plasmonic emission enhancement of quantum dots via plasmonic metafilms. *Nanoscale* **2018**, *10*, 4825–4832.
- (11) Sadeghi, S. M.; Wing, W. J.; Gutha, R. R.; Goul, R. W.; Wu, J. Z. Functional Metal-oxide Plasmonic Metastructures: Ultrabright Semiconductor Quantum Dots with Polarized Spontaneous Emission and Suppressed Auger Recombination. *Phys. Rev. Appl.* **2019**, *11*, No. 024045.
- (12) Kimura, J.; Uematsu, T.; Maenosono, S.; Yamaguchi, Y. Photoinduced fluorescence enhancement in CdSe/ZnS quantum dot submonolayers sandwiched between insulating layers: influence of dot proximity. *J. Phys. Chem. B* **2004**, *108*, 13258–13264.
- (13) Uematsu, T.; Maenosono, S.; Yamaguchi, Y. Photoinduced fluorescence enhancement in Cd Se/ Zn S quantum dot monolayers: Influence of substrate. *Appl. Phys. Lett.* **2006**, *89*, No. 031910.
- (14) Patty, K.; Sadeghi, S. M.; Nejat, A.; Mao, C. B. Enhancement of emission efficiency of colloidal CdSe quantum dots on silicon substrate via an ultra-thin layer of aluminum oxide. *Nanotechnology* **2014**, *25*, 155701.
- (15) Patty, K.; Sadeghi, S. M.; Campbell, Q.; Hamilton, N.; West, R. G.; Mao, C. Probing the structural dependency of photoinduced properties of colloidal quantum dots using metal-oxide photo-active substrates. *J. Appl. Phys.* **2014**, *116*, 114301.
- (16) Sadeghi, S. M.; West, R. G.; Nejat, A. Photo-induced suppression of plasmonic emission enhancement of CdSe/ZnS quantum dots. *Nanotechnology* **2011**, 22, 405202.
- (17) Sadeghi, S. M.; Nejat, A.; Weimer, J. J.; Alipour, G. Chromium-oxide enhancement of photo-oxidation of CdSe/ZnS quantum dot solids. *J. Appl. Phys.* **2012**, *111*, No. 084308.
- (18) Sadeghi, S. M.; Wing, W. J.; Gutha, R. R.; Capps, L. Control of spontaneous emission of quantum dots using correlated effects of metal oxides and dielectric materials. *Nanotechnology* **2017**, 28, No. 095701.
- (19) Sadeghi, S. M.; Nejat, A.; West, R. G. Inhibition of plasmonically enhanced interdot energy transfer in quantum dot solids via photo-oxidation. *J. Appl. Phys.* **2012**, *112*, 104302.
- (20) Zhang, N.; Han, C.; Xu, Y.-J.; Foley, J. J., IV; Zhang, D.; Codrington, J.; Gray, S. K.; Sun, Y. Near-field dielectric scattering promotes optical absorption by platinum nanoparticles. *Nat. Photonics* **2016**, *10*, 473.
- (21) Zhang, N.; Han, C.; Fu, X.; Xu, Y.- J. Function-oriented engineering of metal-based nanohybrids for photoredox catalysis: exerting plasmonic effect and beyond. *Chem.* **2018**, *4*, 1832–1861.
- (22) Han, C.; Li, S.-H.; Tang, Z.-R.; Xu, Y.-J. Tunable plasmonic core—shell heterostructure design for broadband light driven catalysis. *Chem. Sci.* **2018**, *9*, 8914—8922.
- (23) Zhang, N.; Qi, M.-Y.; Yuan, L.; Fu, X.; Tang, Z.-R.; Gong, J.; Xu, Y.-J. Broadband Light Harvesting and Unidirectional Electron Flow for Efficient Electron Accumulation for Hydrogen Generation. *Angew. Chem.* **2019**, *131*, 10108–10112.
- (24) Han, C.; Quan, Q.; Chen, H. M.; Sun, Y.; Xu, Y.-J. Progressive Design of Plasmonic Metal—Semiconductor Ensemble toward Regulated Charge Flow and Improved Vis—NIR-Driven Solar-to-Chemical Conversion. *Small* **2017**, *13*, 1602947.
- (25) Jain, P. K.; Lee, K. S.; El-Sayed, I. H.; El-Sayed, M. A. Calculated absorption and scattering properties of gold nanoparticles of different size, shape, and composition: applications in biological imaging and biomedicine. *J. Phys. Chem. B* **2006**, *110*, 7238–7248.
- (26) Zhang, X.; Chen, Y. L.; Liu, R.-S.; Tsai, D. P. Plasmonic photocatalysis. *Rep. Prog. Phys.* 2013, 76, No. 046401.

- (27) Wang, P.; Huang, B.; Dai, Y.; Whangbo, M.-H. Plasmonic photocatalysts: harvesting visible light with noble metal nanoparticles. *Phys. Chem. Chem. Phys.* **2012**, *14*, 9813–9825.
- (28) Gattinoni, C.; Michaelides, A. Atomistic details of oxide surfaces and surface oxidation: the example of copper and its oxides. *Surf. Sci. Rep.* **2015**, *70*, 424–447.
- (29) Keil, P.; Lützenkirchen-Hecht, D.; Frahm, R. Investigation of room temperature oxidation of Cu in air by Yoneda-XAFS. *AIP Conf. Proc.* **2006**, 490–492.
- (30) Platzman, I.; Brener, R.; Haick, H.; Tannenbaum, R. Oxidation of Polycrystalline Copper Thin Films at Ambient Conditions. *J. Phys. Chem. C* **2008**, *112*, 1101–1108.
- (31) Su, J.; Liu, Y.; Jiang, M.; Zhu, X. Oxidation of copper during physical sputtering deposition: mechanism, avoidance and utilization. *arXivar*, 2014, 1412.2031. DOI: 10.1007/s40843-016-0125-y.
- (32) Drobny, V.; Pulfrey, L. Properties of reactively-sputtered copper oxide thin films. *Thin Solid Films* **1979**, *61*, 89–98.
- (33) Choudhary, S.; Sarma, J.; Pande, S.; Ababou-Girard, S.; Turban, P.; Lepine, B.; Gangopadhyay, S. Oxidation mechanism of thin Cu films: A gateway towards the formation of single oxide phase. *AIP Adv.* **2018**, *8*, No. 055114.
- (34) Hoex, B.; Heil, S.; Langereis, E.; Van de Sanden, M.; Kessels, W. Ultralow surface recombination of c-Si substrates passivated by plasma-assisted atomic layer deposited Al 2 O 3. *Appl. Phys. Lett.* **2006**, *89*, No. 042112.
- (35) Janczarek, M.; Kowalska, E. On the origin of enhanced photocatalytic activity of copper-modified titania in the oxidative reaction systems. *Catalysts* **2017**, *7*, 317.
- (36) Kanninen, P.; Johans, C.; Merta, J.; Kontturi, K. Influence of ligand structure on the stability and oxidation of copper nanoparticles. *J. Colloid Interface Sci.* **2008**, *318*, 88–95.
- (37) Pastoriza-Santos, I.; Sánchez-Iglesias, A.; Rodríguez-González, B.; Liz-Marzán, L. M. Aerobic synthesis of Cu nanoplates with intense plasmon resonances. *Small* **2009**, *5*, 440–443.
- (38) Singh, M.; Sinha, I.; Premkumar, M.; Singh, A.; Mandal, R. Structural and surface plasmon behavior of Cu nanoparticles using different stabilizers. *Colloids Surf.*, A **2010**, 359, 88–94.
- (39) Barreca, D.; Fornasiero, P.; Gasparotto, A.; Gombac, V.; Maccato, C.; Montini, T.; Tondello, E. The potential of supported Cu2O and CuO nanosystems in photocatalytic H2 production. *ChemSusChem* **2009**, *2*, 230–233.
- (40) Scuderi, V.; Amiard, G.; Boninelli, S.; Scalese, S.; Miritello, M.; Sberna, P.; Impellizzeri, G.; Privitera, V. Photocatalytic activity of CuO and Cu2O nanowires. *Mater. Sci. Semicond. Process.* **2016**, 42, 89–93
- (41) Pillai, U. R.; Deevi, S. Room temperature oxidation of carbon monoxide over copper oxide catalyst. *Appl. Catal., B* **2006**, *64*, 146–151
- (42) Lee, J.-S.; Katoch, A.; Kim, J.-H.; Kim, S. S. Effect of Au nanoparticle size on the gas-sensing performance of p-CuO nanowires. *Sens. Actuators, B* **2016**, 222, 307–314.
- (43) Arca, E.; McInerney, M. A.; Shvets, I. V. Band alignment at the interface between Ni-doped Cr2O3 and Al-doped ZnO: implications for transparent p—n junctions. *J. Phys.: Condens. Matter* **2016**, 28, 224004
- (44) Xu, S.; Jacobs, R. M.; Nguyen, H. M.; Hao, S.; Mahanthappa, M.; Wolverton, C.; Morgan, D. Lithium transport through lithium-ion battery cathode coatings. *J. Mater. Chem. A* **2015**, *3*, 17248–17272.
- (45) Bhattacharjee, A.; Ahmaruzzaman, M. CuO nanostructures: facile synthesis and applications for enhanced photodegradation of organic compounds and reduction of p-nitrophenol from aqueous phase. RSC Adv. 2016, 6, 41348–41363.
- (46) Vaidehi, D.; Bhuvaneshwari, V.; Bharathi, D.; Sheetal, B. P. Antibacterial and photocatalytic activity of copper oxide nanoparticles synthesized using Solanum lycopersicum leaf extract. *Mater. Res. Express* **2018**, *5*, No. 085403.
- (47) Pan, Z.; Zhao, K.; Wang, J.; Zhang, H.; Feng, Y.; Zhong, X. Near infrared absorption of CdSe x Te1-x alloyed quantum dot

- sensitized solar cells with more than 6% efficiency and high stability. *ACS Nano* **2013**, *7*, 5215–5222.
- (48) Zhao, G.; Wang, W.; Bae, T.-S.; Lee, S.- G.; Mun, C.; Lee, S.; Yu, H.; Lee, G.-H.; Song, M.; Yun, J. Stable ultrathin partially oxidized copper film electrode for highly efficient flexible solar cells. *Nat. Commun.* **2015**, *6*, 8830.
- (49) Kondo, J.; et al. Cu 2 O as a photocatalyst for overall water splitting under visible light irradiation. *Chem. Commun.* 1998, 357–358
- (50) Sharma, P.; Sharma, S. K. Photocatalytic degradation of cuprous oxide nanostructures under UV/Visible irradiation. *Water Resour. Manag.* **2012**, *26*, 4525–4538.
- (51) Yu, Y.; Zhao, Y.; Sun, H.; Ahmad, M. Au nanoparticles decorated CuO nanowire arrays with enhanced photocatalytic properties. *Mater. Lett.* **2013**, *108*, 41–45.
- (52) Chakraborty, P.; Dhar, S.; Debnath, K.; Majumder, T.; Mondal, S. P. Non-enzymatic and non-invasive glucose detection using Au nanoparticle decorated CuO nanorods. *Sens. Actuators, B* **2019**, 283, 776–785.
- (53) Pan, Y.; Deng, S.; Polavarapu, L.; Gao, N.; Yuan, P.; Sow, C. H.; Xu, Q.-H. Plasmon-enhanced photocatalytic properties of Cu2O nanowire—Au nanoparticle assemblies. *Langmuir* **2012**, *28*, 12304—12310.
- (54) Kwon, J.; Cho, H.; Jung, J.; Lee, H.; Hong, S.; Yeo, J.; Han, S.; Ko, S. ZnO/CuO/M (M= Ag, Au) Hierarchical Nanostructure by Successive Photoreduction Process for Solar Hydrogen Generation. *Nanomaterials* **2018**, *8*, 323.
- (55) Sadeghi, S.; Hatef, A.; Nejat, A.; Campbell, Q.; Meunier, M. Plasmonic emission enhancement of colloidal quantum dots in the presence of bimetallic nanoparticles. *J. Appl. Phys.* **2014**, *115*, 134315.
- (56) Javier, A.; Magana, D.; Jennings, T.; Strouse, G. F. Nanosecond exciton recombination dynamics in colloidal CdSe quantum dots under ambient conditions. *Appl. Phys. Lett.* **2003**, *83*, 1423–1425.
- (57) Nizamoglu, S.; Demir, H. V. Resonant nonradiative energy transfer in CdSe/ZnS core/shell nanocrystal solids enhances hybrid white light emitting diodes. *Opt. Express* **2008**, *16*, 13961–13968.
- (58) Klimov, V.; McBranch, D.; Leatherdale, C.; Bawendi, M. Electron and hole relaxation pathways in semiconductor quantum dots. *Phys. Rev. B: Condens. Matter Mater. Phys.* **1999**, *60*, 13740.
- (59) Brovelli, S.; Schaller, R. D.; Crooker, S.; García-Santamaría, F.; Chen, Y.; Viswanatha, R.; Hollingsworth, J. A.; Htoon, H.; Klimov, V. I. Nano-engineered electron—hole exchange interaction controls exciton dynamics in core—shell semiconductor nanocrystals. *Nat. Commun.* **2011**, *2*, 280.
- (60) Jones, M.; Lo, S. S.; Scholes, G. D. Quantitative modeling of the role of surface traps in CdSe/CdS/ZnS nanocrystal photoluminescence decay dynamics. *Proc. Natl. Acad. Sci. U. S. A.* **2009**, 106, 3011–3016.
- (61) Jones, M.; Lo, S. S.; Scholes, G. D. Signatures of exciton dynamics and carrier trapping in the time-resolved photoluminescence of colloidal CdSe nanocrystals. *J. Phys. Chem. C* **2009**, *113*, 18632–18642.
- (62) Chang, C.-L.; Sankaranarayanan, S. K.; Engelhard, M. H.; Shutthanandan, V.; Ramanathan, S. On the relationship between nonstoichiometry and passivity breakdown in ultrathin oxides: combined depth-dependent spectroscopy, Mott-Schottky analysis, and molecular dynamics simulation studies. *J. Phys. Chem. C* **2009**, 113, 3502–3511.